Conjugate Thermal Simulation for Sheet Extrusion Die

Hong Yang
Nordson EDI, Chippewa Falls, Wisconsin 54729

The thermal effects on manifold temperature uniformity and output flow uniformity are important for polymer extrusion die design. Lin and Jaluria (Lin and Jaluria, *Polym. Eng. Sci*., 37, 1582 (1997)) has carried out a numerical study on conjugate heat transfer for extrusion polymer flow under the assumption that the die body surface is in uniform temperature or heat transfer coefficient. In this study, we have solved the non-uniform body surface temperature as part of the simulation solutions based on heat flux boundary conditions (including radiation and convection heat transfer). The body temperature is computed in conjugated with the melt polymer flow with non-linear viscous shear heating effect. The relative tough thermal conditions are set to test uniformity of the temperature distribution on the manifold wall. We also give the results of the heat transfer effect on the flow velocity distribution. POLYM. ENG. SCI., 54:682–694, 2014. © 2013 Society of Plastics Engineers

INTRODUCTION

A sheet extrusion die is the workhorse of the plastic film and sheet industry. A high level of output uniformity at the die exit as well as product throughput is critical in practice [1]. To guarantee distribution uniformity of output product, temperature uniformity on the manifold wall is a crucial design criterion for flat extrusion die. The design challenge for temperature control on manifold wall is that the die body temperature is non-uniform and coupled with highly viscous molten polymer flow inside. Lin and Jaluria [2] has carried out a numerical study on conjugate heat transfer for the extrusion polymer flow under the assumption that the die body surface is in uniform temperature or heat transfer coefficient. However, temperature or heat transfer coefficient on die body surface cannot be uniform in reality, and can vary at a large range due to heat loss via radiation or convection or heater source. It is necessary to understand how the varying body temperature can affect temperature of the manifold channel wall on which the molten polymer flows. So far this question has not been thoroughly answered yet from reliable 3D simulation. Also the die body temperature (including the surface temperature) should be a part of the solution of the whole problem. Therefore, it is particularly interesting to explore the effects of various body thermal boundary conditions on temperature distribution on manifold wall and the flow velocity field in conjugate with the melt polymer flow of different viscosity. To establish useful design principles, it is also necessary to study detailed geometry configurations and heat transfer between contour body, heaters, flex bar, and bolts, etc. In order to give reliable data, all the above simulations should be based on accuracy-preserved solvers.

In this study, we present detailed conjugate thermal simulations and analysis based on the 3D finite element solver, ANSYS POLYFLOW [3] including its heat conduction solver. The rest of the study is organized as follows. Firstly, accuracy of the heat conduction solver is tested. Next in the section of computational model, we discuss material properties, geometry and mesh generation, and various boundary conditions. Then the results are analyzed. Finally, the conclusions and design optimizations are given.

ACCURACY TEST

Even though the commercial package ANSYS POLYFLOW and its related heat conduction solver have been developed for some years, it is still worthwhile to test its accuracy from a user's viewpoint in order to build up the customers' confidence on the present simulation results. Here we only focus on the heat conduction solver for our thermal simulation purpose.

Consider a regular cylindrical solid with length $L=12$ inch and constant cross section area. A coarse mesh (Fig. 1a) is used for testing. A thermal insulation boundary condition is applied on its side wall and temperature on the inlet circular face (left) is set to $T_{\text{inlet}}=520\,F$. For the right outlet face, we set:

Case 1: Temperature $T_{\text{outlet}} = 400\,F$.

Case 2: Heat cooling:

$$Q_{\text{outlet}} = 0.5\sigma[(T+T_0)^4 - (80+T_0)^4]$$

where

$$\sigma = 5.6703 \times 10^8 \frac{W}{m^2 \text{J} K^4},\ T_0 = 459.67\,F. \qquad (1)$$

Correspondence to: Hong Yang; e-mail: hongyang101@gmail.com
DOI 10.1002/pen.23609
Published online in Wiley Online Library (wileyonlinelibrary.com).

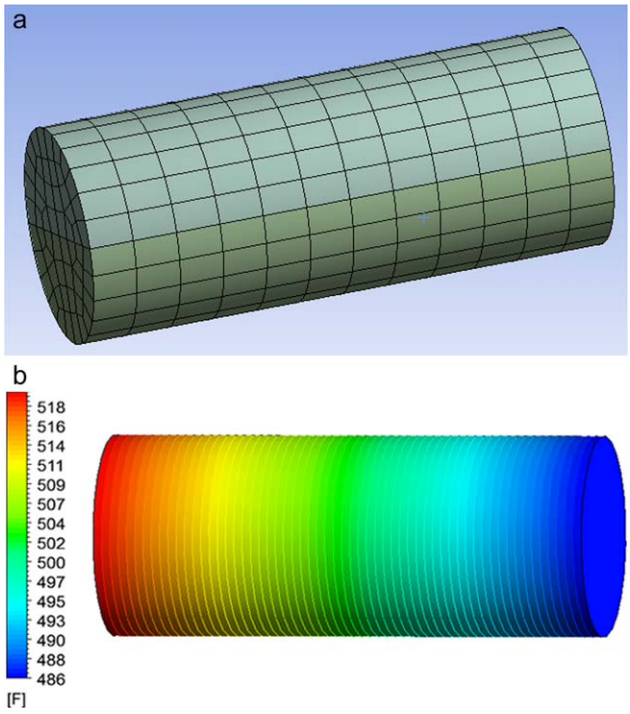

FIG. 1. (a,b) Accuracy test on cylinder. [Color figure can be viewed in the online issue, which is available at wileyonlinelibrary.com.]

In Case 1, the exact temperature gradient, ∂T, is constant. To compare with its exact solution, we define the L_1 and L_∞ error norms for temperature gradient as follows:

$$L_1 \text{ error norm} = \frac{|\partial \bar{T} - \partial T_{\text{exact}}|}{\partial T_{\text{exact}}},$$
$$L_\infty \text{ error norm} = \frac{|\partial T_{\text{outlet}} - \partial T_{\text{exact}}|}{\partial T_{\text{exact}}}. \quad (2)$$

Here $\partial \bar{T}$, $\partial T_{\text{outlet}}$, $\partial T_{\text{exact}}$ are the average gradient, gradient at the outlet, and the exact gradient solution, respectively. The resulted L_1 and L_∞ error norms for temperature gradient are 6.8 e^{-8} and 1.0 e^{-7}, respectively.

In Case 2, (Fig. 1b), T_{outlet}=485.851 F, thus the relative heat flux error is 7.0 e^{-6}.

The above small errors close to machine round-off errors show that the heat conduction solver indeed preserves accuracy well enough for second-order accuracy simulation as expected.

COMPUTATIONAL MODEL

Material Properties

Polybutylene terephthalate (PBT) and linear low-density polyethylene (LLDPE) are used as example resins to cover the wide range of viscosity that the same contour die can handle.

The viscosity of the melt polymer depends on temperature and shear rate, which can be modeled as modified cross model based on approximate Arrhenius shear stress:

$$\eta = \frac{\eta_0}{1 + (\eta_0 \dot{\gamma} H(T)/\tau^*)^{1-n}} . H(T), \quad (3)$$
$$H(T) = e^{-\beta(T-T_p)}. \quad (4)$$

For LLDPE: $\eta_0 = 3.388744 \times 10^2$ Poise, $\tau^* = 8.828441 \times 10^5$ Pa, $n = 0.245447$, $\beta = 0.03$. In melt state, density $\rho = 0.74$ g/cc, operating temperature $T_p = 490\,F$.

For PBT: $\eta_0 = 8.186826 \times 10^2$ Poise, $\tau^* = 4.172760 \times 10^6$ Pa, $n = 0.296856$, $\beta = 0.05$. In melt state, density $\rho = 0.91$ g/cc, operating temperature $T_p = 482\,F$.

The above η_0, τ^*, n, β are curve fitting constants based on experimental data from Fig. 2a–c. To show uniformity of flow temperature even in a tough scenario, first we consider flow viscosity independent of temperature by setting $\beta = 0$, then we give the flow field comparisons by including temperature dependency for viscosity of the PBT. Also for the same purpose of testing manifold temperature in a tough situation, we are more interesting in PBT because it has higher viscosity value than LLDPE, thus PBT could bring more viscous shear heating to give more temperature variation on the manifold wall.

The conductivity for the die body and polymer resin is set to be 30 and 0.15 W/m K, respectively. The specific heat for polymer flow is set to be 2 J/g K.

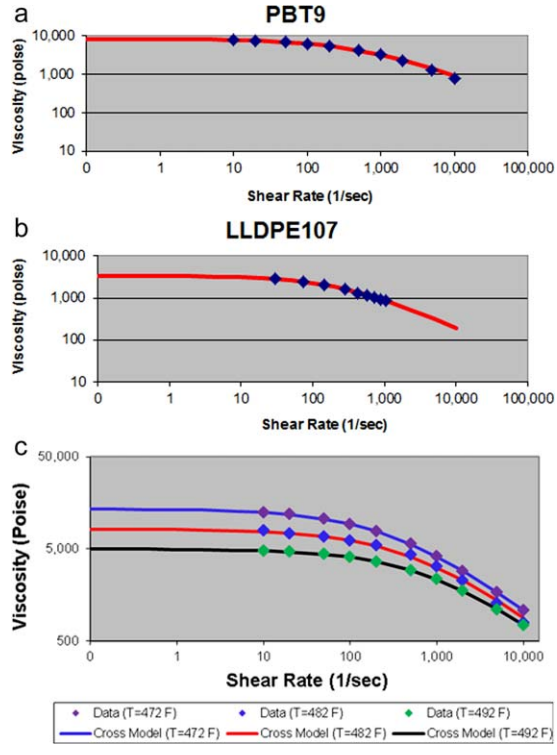

FIG. 2. (a–c) Viscosity. [Color figure can be viewed in the online issue, which is available at wileyonlinelibrary.com.]

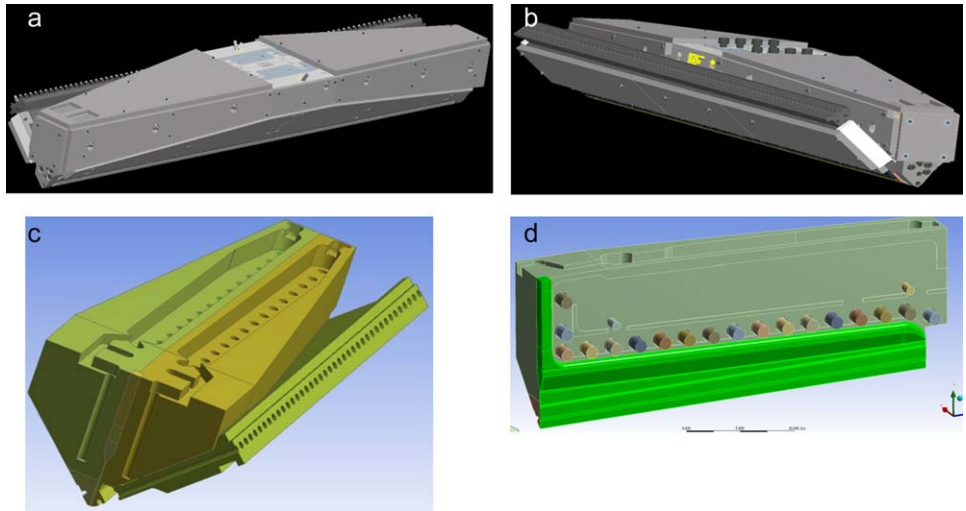

FIG. 3. (a–d) Geometry. [Color figure can be viewed in the online issue, which is available at wileyonlinelibrary.com.]

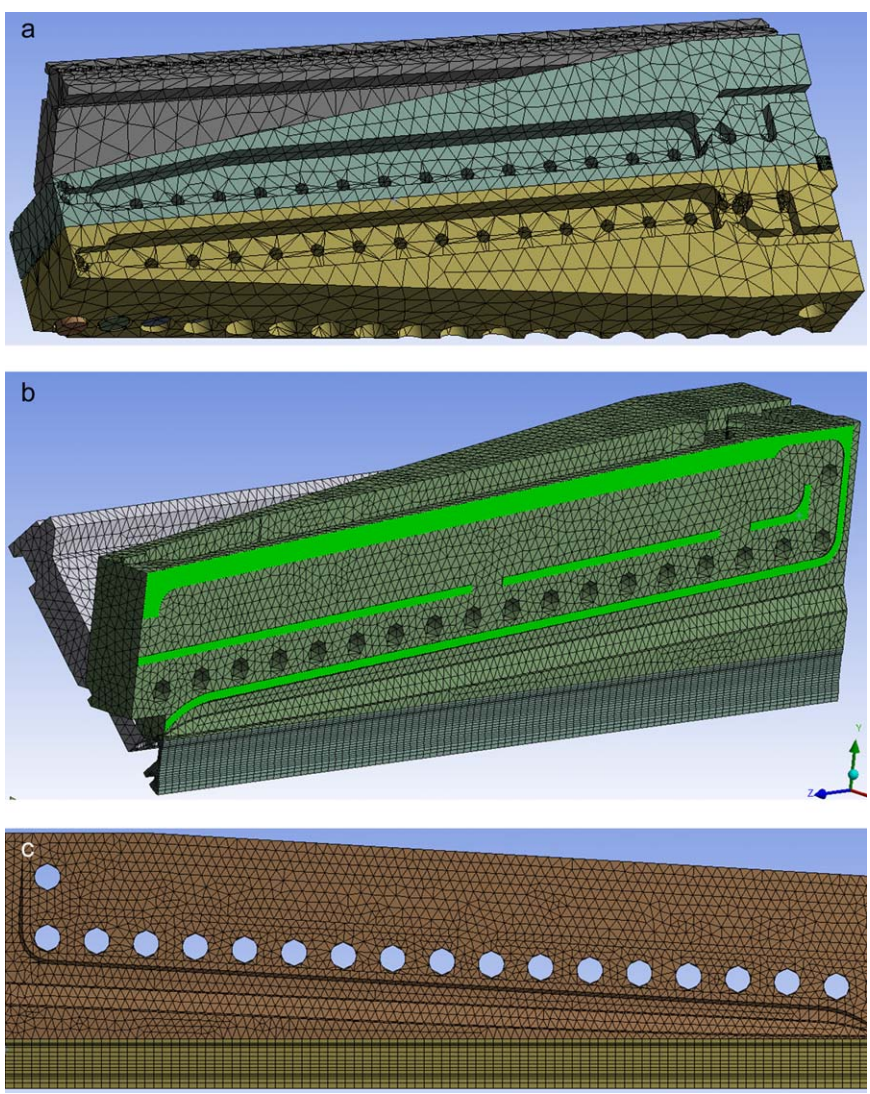

FIG. 4. (a–c) Dies body mesh. [Color figure can be viewed in the online issue, which is available at wileyonlinelibrary.com.]

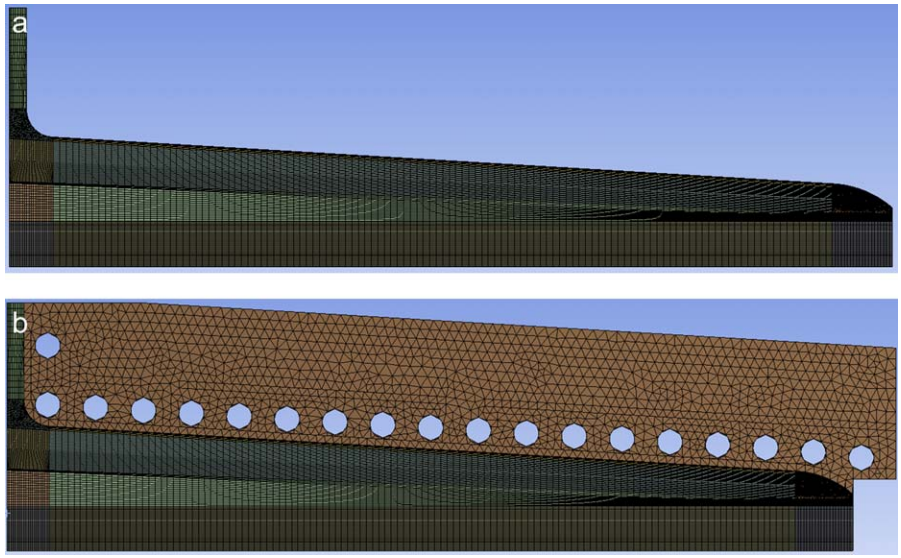

FIG. 5. (a,b) Flow domain mesh. [Color figure can be viewed in the online issue, which is available at wileyonlinelibrary.com.]

Geometry and Mesh

A production contour die of 88.6-inch long with heater box, body bolts, and AutoFlex® bar (Fig. 3a and b) is used for the present simulations. The geometry (Fig. 3c) is stored in CAD Parasolid file format. Due to symmetry, only half of the die is computed, where the manifold is in green color (Fig. 3d). For the solid part, a mixed tetrahedral-hexahedral mesh with about 284,000 elements was generated (Fig. 4a–c) for the die body to represent all the geometry details including die body, heater holes, body bolts and holes, heater box, detailed flex bar, sealing faces, etc. Here the sealing faces are meshed in green color. Here the hexahedral mesh is used in the lower part of the die body to give topologically conformal mesh with the manifold mesh on the pre-land, secondary and lip land walls.

The flow domain is the corresponding manifold inside the die (Fig. 3d). A conformal hexahedral-dominant mesh with about 187,000 elements (Fig. 5a) was generated to accurately represent temperature gradient near the wall, particularly for 3D curved wall surfaces. Figure 5b shows this flow domain mesh together with the body mesh.

In order to reduce interpolation error and thus avoid temperature oscillations on the interface of the fluid and solid, fine meshes for both the flow domain and the die body have been generated and refined to get accuracy-converged results. Moreover, the meshes on the wall boundary of the flow domain (Fig. 5a) have been generated to be finer than the body manifold meshes (Fig. 4c) to address the non-linear viscous shear heating problem.

Boundary Conditions

For thermal boundary conditions, we set a much tougher thermal situation than in practical operation to test the results on temperature uniformity. Only one heater zone is set, that is, the same constant (die operation) temperature for all the body heaters. In reality, there are 14 body heater zones with dynamic temperature control through the thermocouples on the die. The two lip heaters are modeled by using the constant die operation temperature.

Detailed natural convection heat loss is assumed for each body face. For air natural convection, the Rayleigh number is calculated from the Grashof and Prandtl number:

$$Ra = GrPr = \frac{g\beta(T_s - T_\infty)L^3}{\upsilon^2}Pr \tag{5}$$

where $g = 9.8\,m/s^2, \beta = 2/(T_\infty + T_s), \upsilon = 1.65 \times 10^{-5}$ m^2/s, $Pr = 0.7$, and L is characteristic length for a plate

TABLE 1. Heat transfer coefficients.

Boundary face	$\alpha\,(lbs^{-3}F)$	$T_\alpha(F)$	$T_\alpha(F)$
Flex bar face #1	24.3	150	150
AutoFlex face #2	12.1	75	75
AutoFlex face #3	18.9	75	75
Bolt face top	20	75	75
End block face #1	14.4	75	75
Fix body face #1	13.5	75	75
Fix body face #2	14	75	75
Fix body face #3	15	75	75
Fix body face #4	18.9	75	75
Flex body face #1	16.3	75	75
Flex body face #2	18.6	75	75
Flex body face #3	21	75	75
Flex body face #4	25.9	200	200
Wire box face #1	23.6	75	75
Wire box face #2	0	0	75

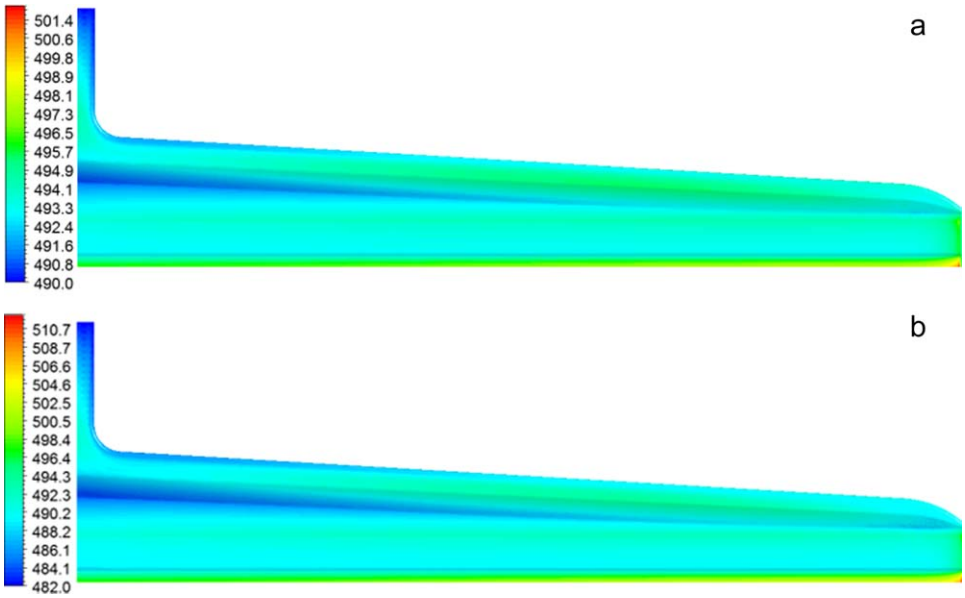

FIG. 6. (a) Temperature on adabatic flow boundary surfaces (LLDPE) and (b) temperature on adabatic flow boundary surfaces (PBT). [Color figure can be viewed in the online issue, which is available at wileyonlinelibrary.com.]

surface. The Nusselt numbers are found from the correlations given in [4] for each surfaces. For vertical surface,

$$\mathrm{Nu}=\begin{cases} 0.59\,Ra^{1/4} & (10^4 < Ra < 10^9) \\ 0.1\,Ra^{1/3} & (10^9 < Ra < 10^{13}) \end{cases} \tag{6}$$

For inclined surfaces, g is replaced by $g\cos\theta$ in (4).

For horizontal surface,
upper side:

$$\mathrm{Nu}=\begin{cases} 0.54\,Ra^{1/4} & (10^4 < Ra < 10^7) \\ 0.15\,Ra^{1/3} & (10^7 < Ra < 10^{11}) \end{cases}, \tag{7}$$

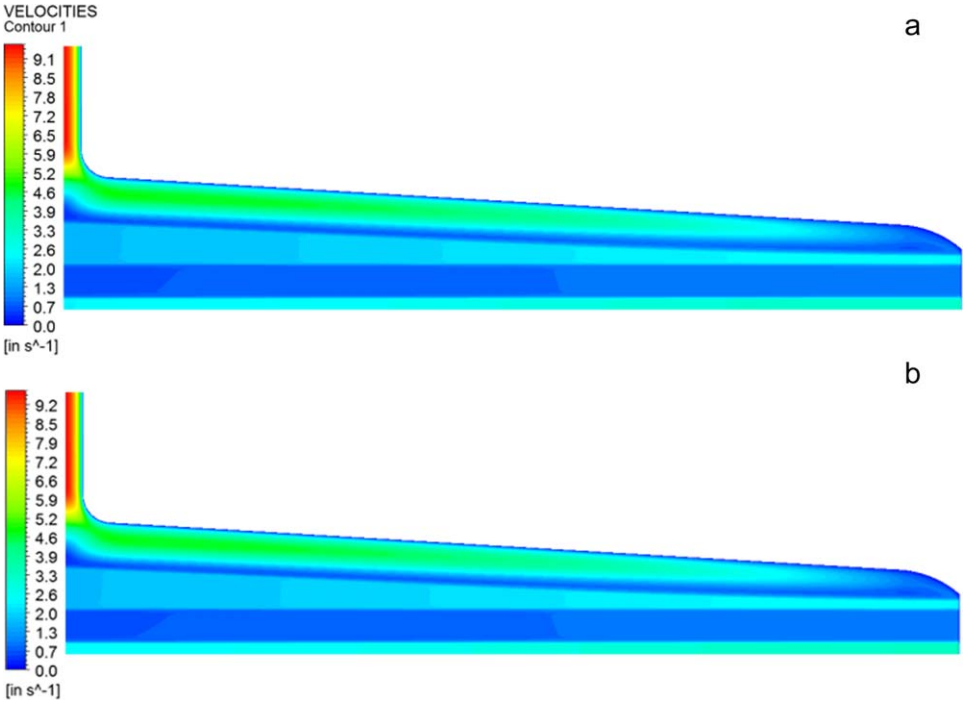

FIG. 7. (a) Velocity on center plane (LLDPE) and (b) Velocity on center plane (PBT). [Color figure can be viewed in the online issue, which is available at wileyonlinelibrary.com.]

 DOI 10.1002/pen

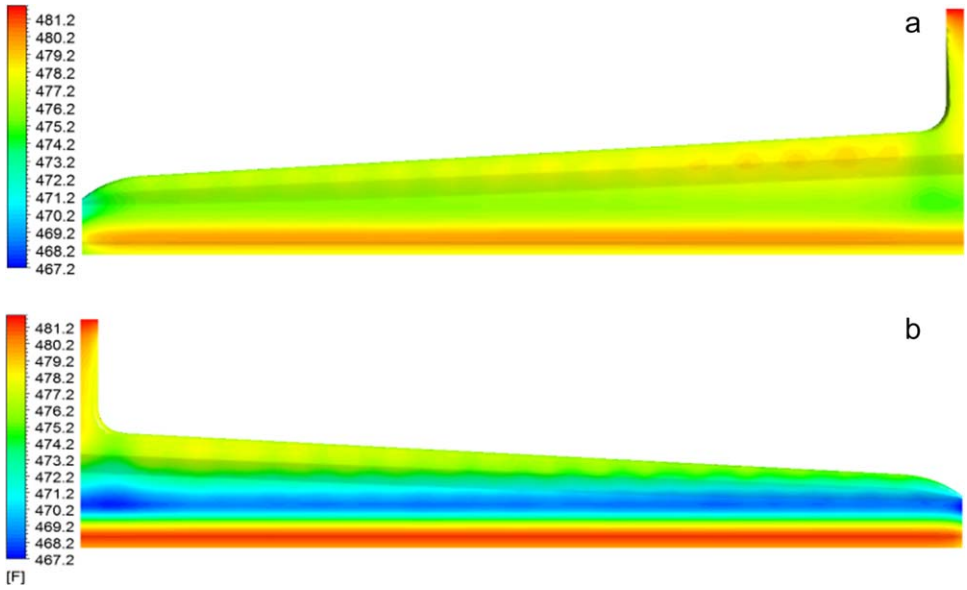

FIG. 8. (a) Temperature on adabatic manifold wall; heat loss case (fix side) and (b) heat loss case (flex side). [Color figure can be viewed in the online issue, which is available at wileyonlinelibrary.com.]

lower side:

$$\mathrm{Nu} = 0.27\,Ra^{1/4} \quad (10^5 < Ra < 10^{11}). \tag{8}$$

As an illustration, Table 1 gives the calculated heat coefficients for a few body surfaces out of more than 30 faces that we have done.

In a real-world installation, the insulation plates (Fig. 3a) are put on the above surfaces to avoid heat loss and give temperature uniformity. Due to the heat flux brought in by the feed block, the middle back surface of the wire box is set to be at the same constant operating temperature in heat loss case.

The overall surface heat flux for face i is formulated in thermal resistance form as follows:

$$q_i = q_c + \alpha(T - T_\alpha) + \epsilon\sigma[(T + T_0)^4 - (T_\sigma + T_0)^4] \tag{9}$$

where T is the body surface temperature to be solved; q_c is the constant input heat flux if any; α, T_α are the Newton convection heat coefficient and ambient air flow temperature, respectively; ε is the body surface

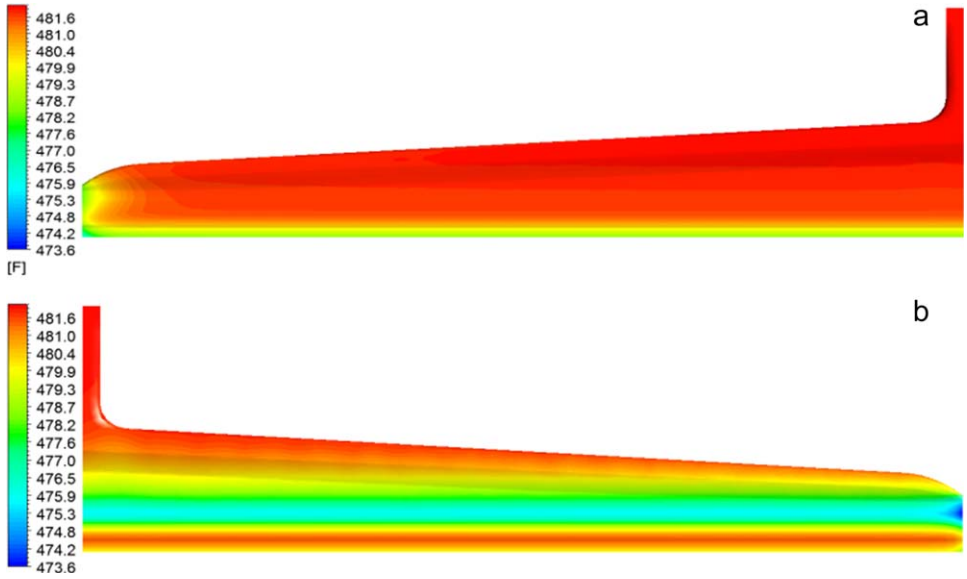

FIG. 9. (b) Temperature on adabatic manifold wall; insulation case (fix side) and (b) insulation case (flex side). [Color figure can be viewed in the online issue, which is available at wileyonlinelibrary.com.]

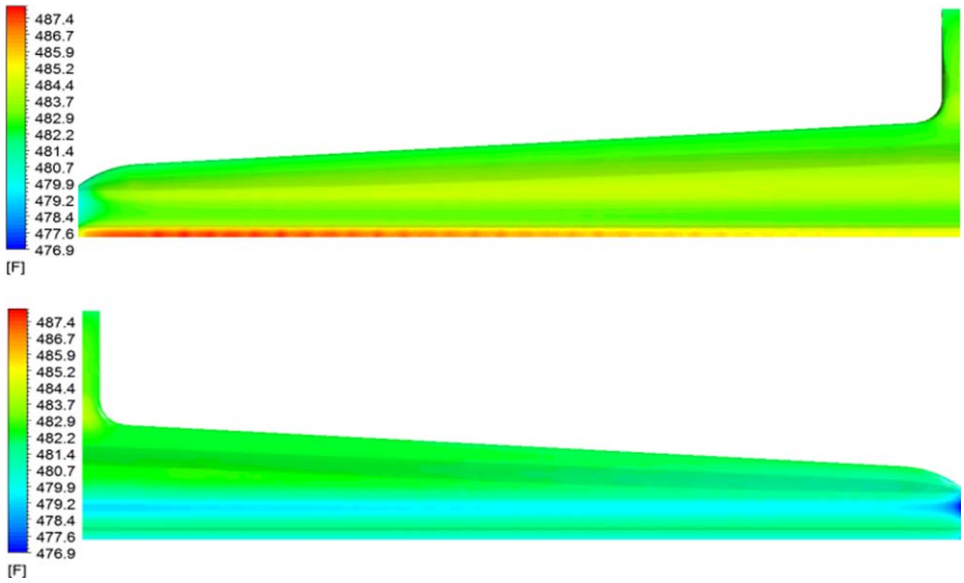

FIG. 10. Temperature on conjugate manifold wall; insulation case (fix side) and (b) insulation case (flex side). [Color figure can be viewed in the online issue, which is available at wileyonlinelibrary.com.]

emissivity; σ and T_0 are the Stefan-Boltzmann constant and base temperature constant, respectively, as given in *Eq. 1*; T_σ is the environmental temperature for radiation.

On the die body surfaces, radiation is the major heat loss while convection is the minor heat loss. Emissivity of typical stainless steel is about $\varepsilon = 0.03 \sim 0.3$, but here we set a much higher emissivity, $\varepsilon = 0.8$ to test temperature uniformity.

The total heat loss to the environment per unit time from the die body surface can be formulated as follows:

$$Q = \sum_{i=0}^{N} q_i A_i, \tag{10}$$

where A_i is the area of face i, and N is the total number of body surfaces.

For the flow motion, we set zero-velocity condition for the manifold wall, symmetry condition for the symmetric cut-plane, outflow condition for the lip exit. The mass flow rate through the half inlet for PBT is 441 lb/h while the mass flow rate for LLDPE is set to be 358.6 lb/h.

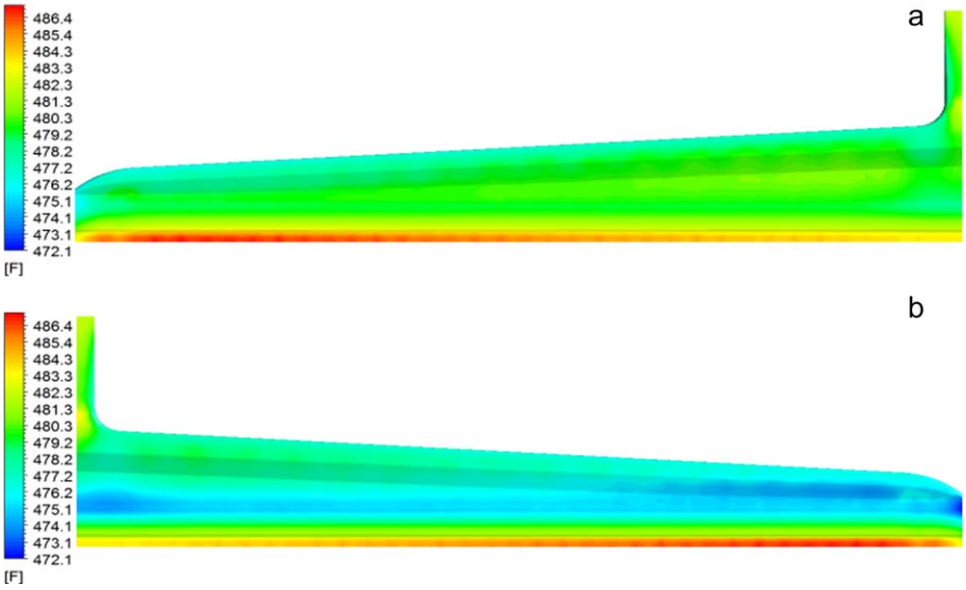

FIG. 11. Temperature on conjugate manifold wall; heat loss case (fix side) and (b) heat loss case (flex side). [Color figure can be viewed in the online issue, which is available at wileyonlinelibrary.com.]

 DOI 10.1002/pen

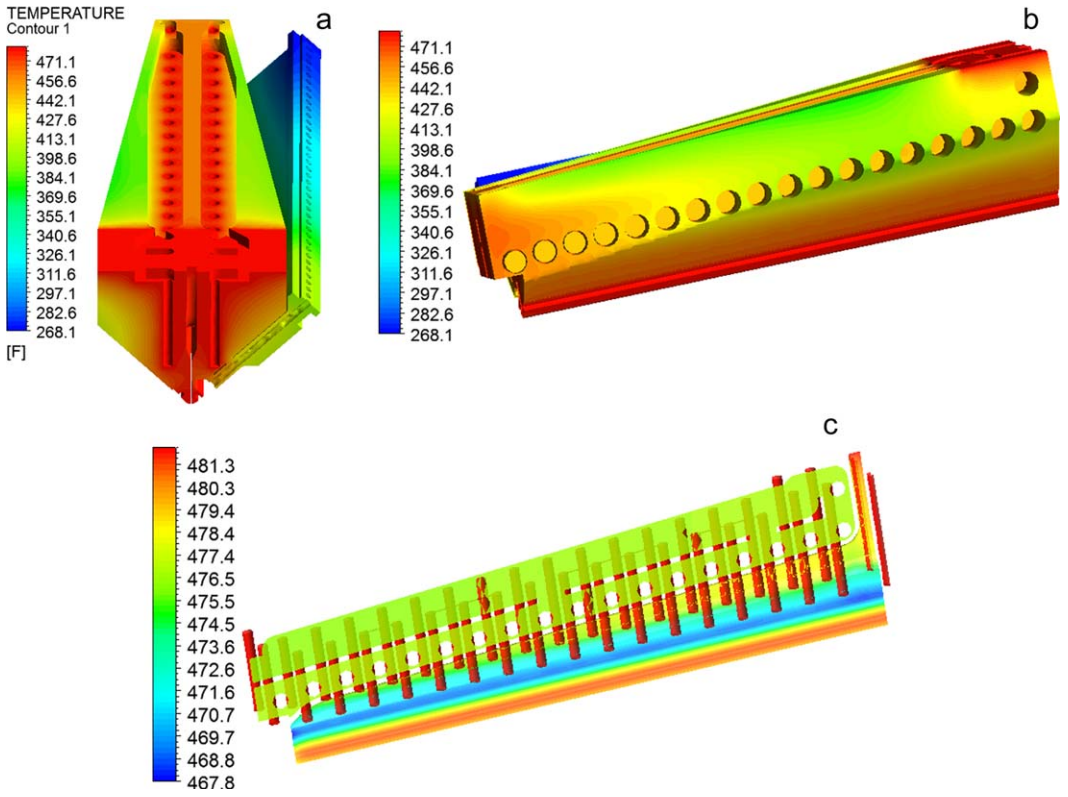

FIG. 12. (a–c) Temperature on body heat loss case–adiabatic manifold. [Color figure can be viewed in the online issue, which is available at wileyonlinelibrary.com.]

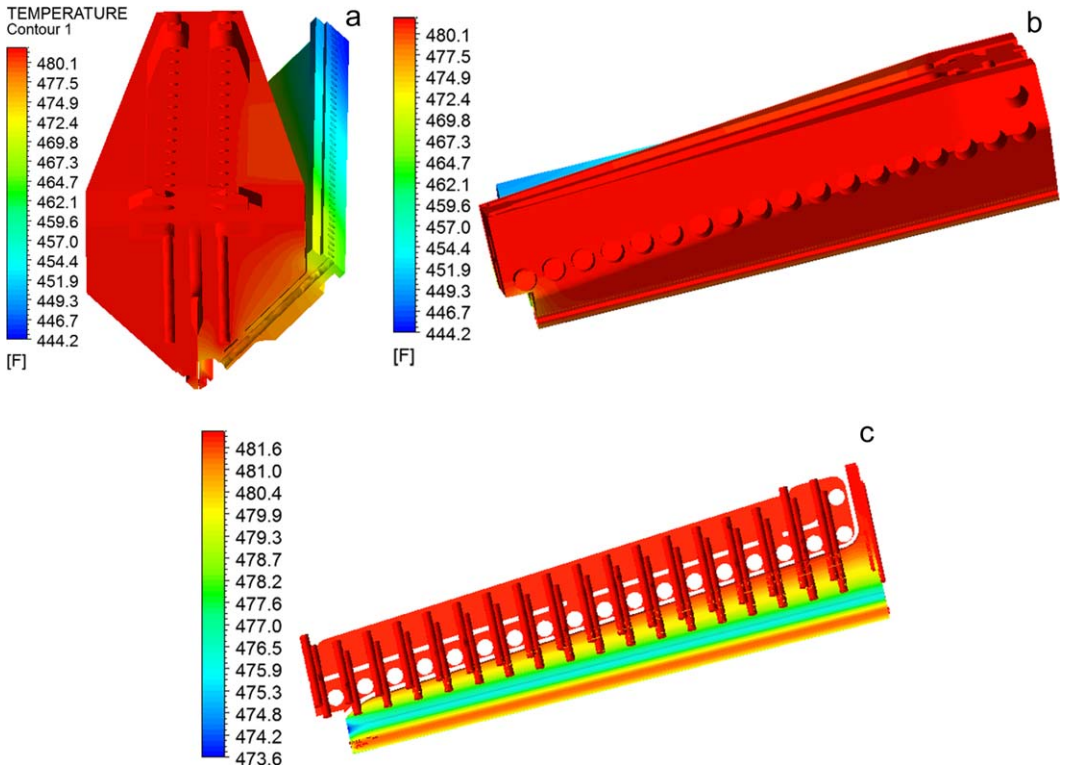

FIG. 13. (a–c) Temperature on body; insulation case; adiabatic manifold. [Color figure can be viewed in the online issue, which is available at wileyonlinelibrary.com.]

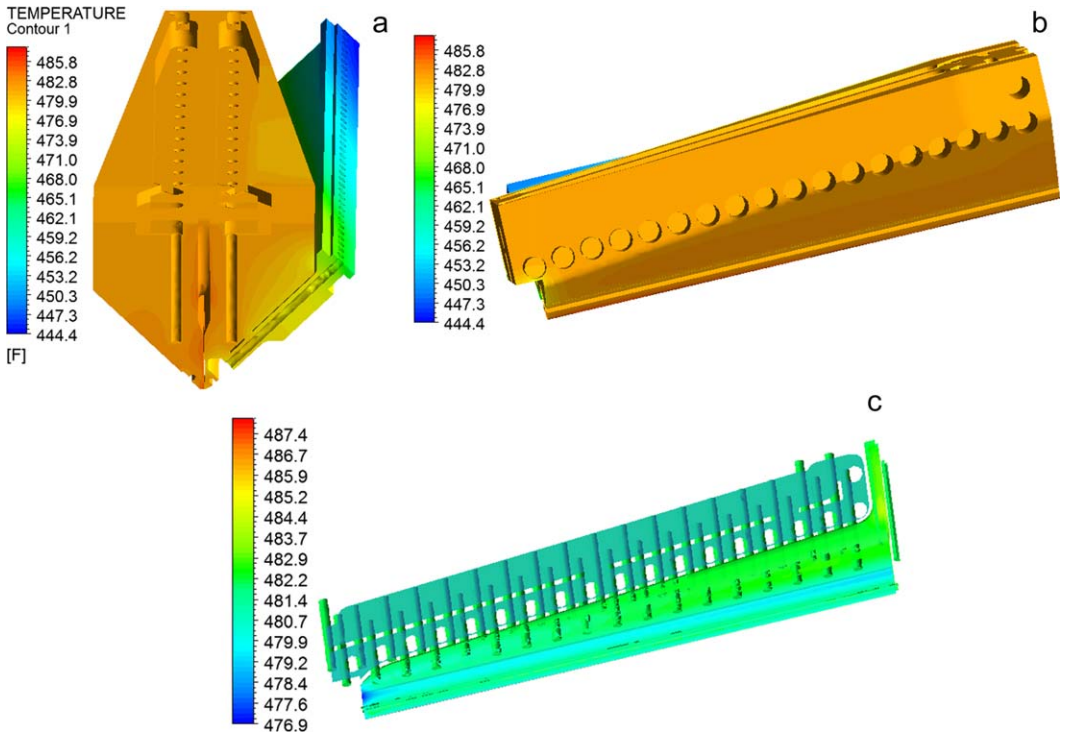

FIG. 14. (a–c) Temperature on body; insulation case; conjugate manifold. [Color figure can be viewed in the online issue, which is available at wileyonlinelibrary.com.]

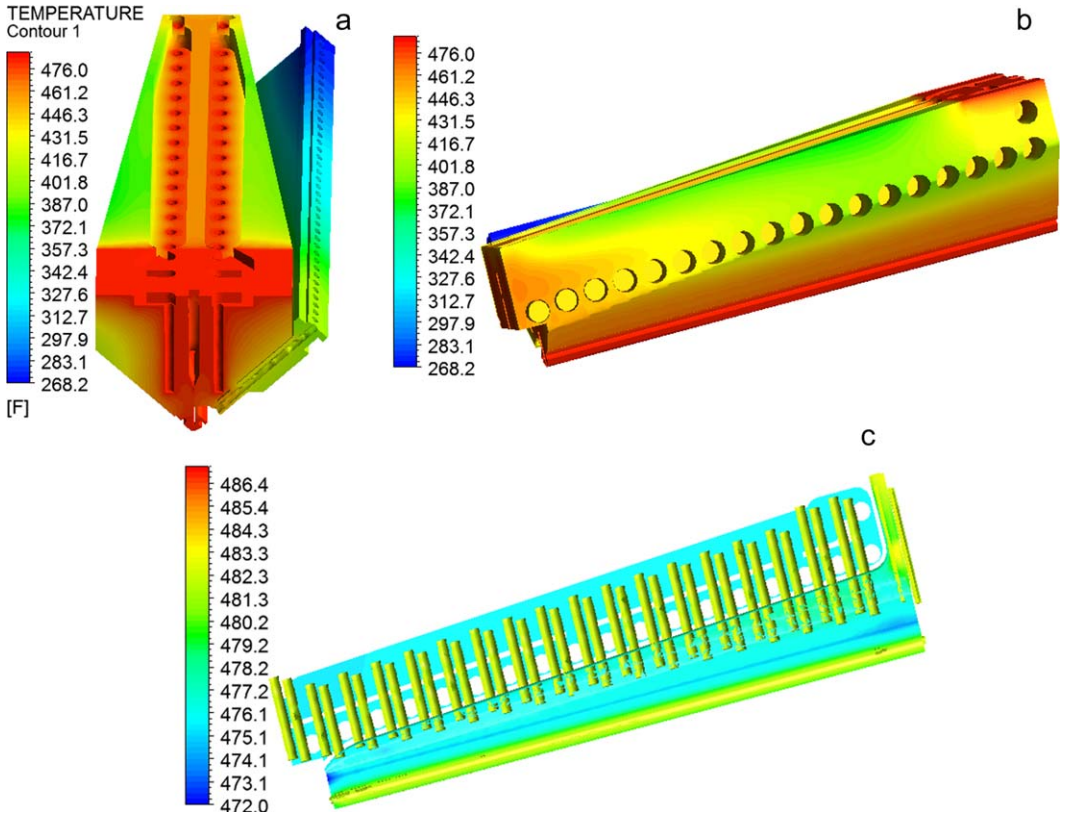

FIG. 15. (a–c) Temperature on body; heat loss case; conjugate-manifold. [Color figure can be viewed in the online issue, which is available at wileyonlinelibrary.com.]

 DOI 10.1002/pen

a

	VELOCITIES	TEMPERATURE
1	1	0.3772
2	0.023384	0.07007
3	0.0022606	0.013471
4	0.0005198	0.00014055
5	0.00012456	2.7304e-005
6	3.2193e-005	4.2252e-006
7	8.8286e-006	5.4842e-007
8	2.4453e-006	1.0999e-007
9	6.823e-007	2.9739e-008
10	1.9148e-007	8.039e-009
11	5.3985e-008	2.3882e-009
12	1.5277e-008	7.9824e-010
13	4.337e-009	2.4936e-010

b

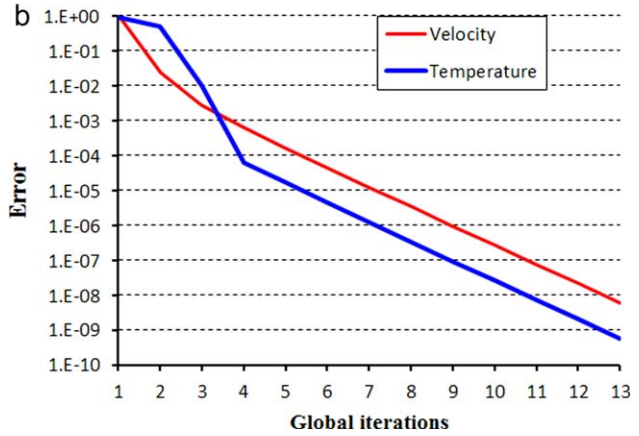

FIG. 16. (a,b) Convergence history. [Color figure can be viewed in the online issue, which is available at wileyonlinelibrary.com.]

Non-isothermal adiabatic and conjugate wall conditions are applied on the manifold wall and flow wall boundaries. The coupled thermal connections (equivalent temperature and zero-leak of heat flux) are also applied as boundary condition between manifold sealing faces, bolt and body connections, flex bar and die body connections.

RESULTS AND DISCUSSIONS

To accurately show manifold temperature uniformity in the same contour die, we have done comprehensive case studies based on converged solutions on the above fine meshes. Recall that we only set up one body heater zone instead of multiple zones (actually 14 zones) in reality in order to give tough test here. The present solutions of velocity and temperature have converged to error norm of less than 10^{-8} as shown in the typical history of convergence in Fig. 16a and b. In terms of manifold temperature uniformity, both good and tough thermal conditions are tested, including effects of viscosity, insulation and non-insulation, adiabatic and conjugate wall.

Figures 6–8, and 12 show the results for the adiabatic manifold wall case with large heat loss to the environment from the die body surfaces. We have computed PBT resin (Figs. 6a and 7a) operating at 482°F with high viscosity and LLDPE (Figs. 6b and 7b) at 490°F with low viscosity. The shear heating results in about 18 and 8°F of temperature change on the adiabatic flow wall boundary for the PBT and LLDPE cases, respectively. Some tiny areas of numerical error noise shown in the graphs can be ignored. The manifold wall temperature (Fig. 8a and b) varies 15°F from 467 to 482°F. This small temperature variation is acceptable considering that heat loss here is enlarged, and that in reality melt temperature

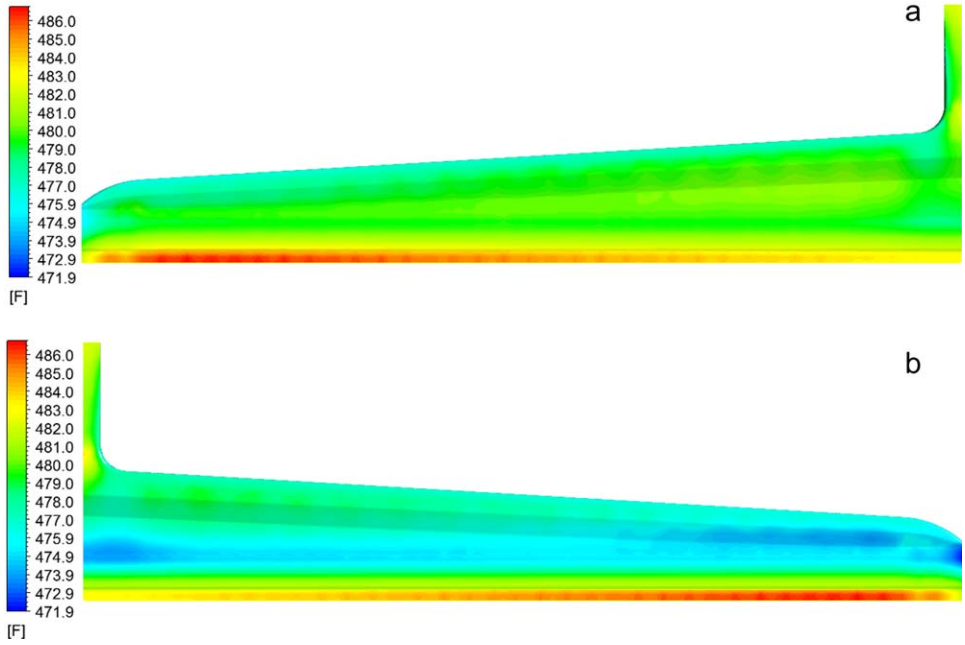

FIG. 17. (a) T-Fix-$H(T)$ and (b) T-Flex-$H(T)$. [Color figure can be viewed in the online issue, which is available at wileyonlinelibrary.com.]

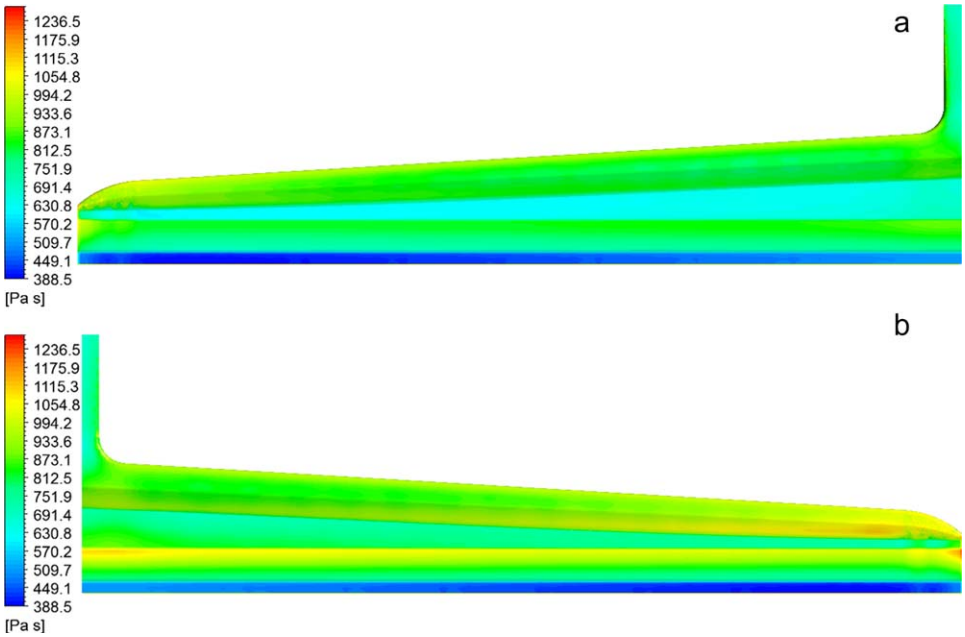

FIG. 18. (a) Viscosity Fix $H(T)$ and (b) viscosity-Flex-$H(T)$. [Color figure can be viewed in the online issue, which is available at wileyonlinelibrary.com.]

distribution at the entrance can be varied at this range. It is noted in Fig. 12a–c that the die body temperature distribution varies in a wide range from 268 to 482°F.

Figures 9 and 13 give the more realistic scenario with insulation plates to avoid heat loss when actually running the contour dies, still assuming adiabatic flow wall boundary here. As expected, the temperature variation of 8°F from 474 to 482°F on the manifold wall (Fig. 9a and b) is smaller than in the previous heat loss case (Fig. 8a and b). Also the body surface temperature variation from 444 to 482°F (Fig. 13a and b) is much smaller than that in the heat loss case (Fig. 12).

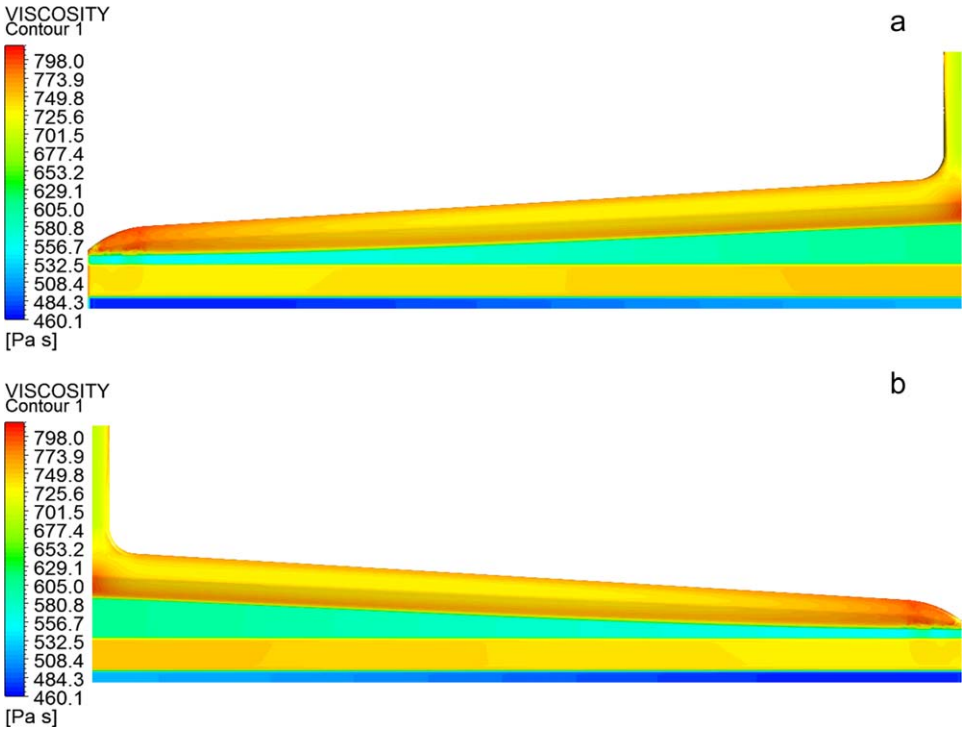

FIG. 19. (a) Viscosity Fix $H = 1$ and (b) viscosity Flex $H = 1$. [Color figure can be viewed in the online issue, which is available at wileyonlinelibrary.com.]

 DOI 10.1002/pen

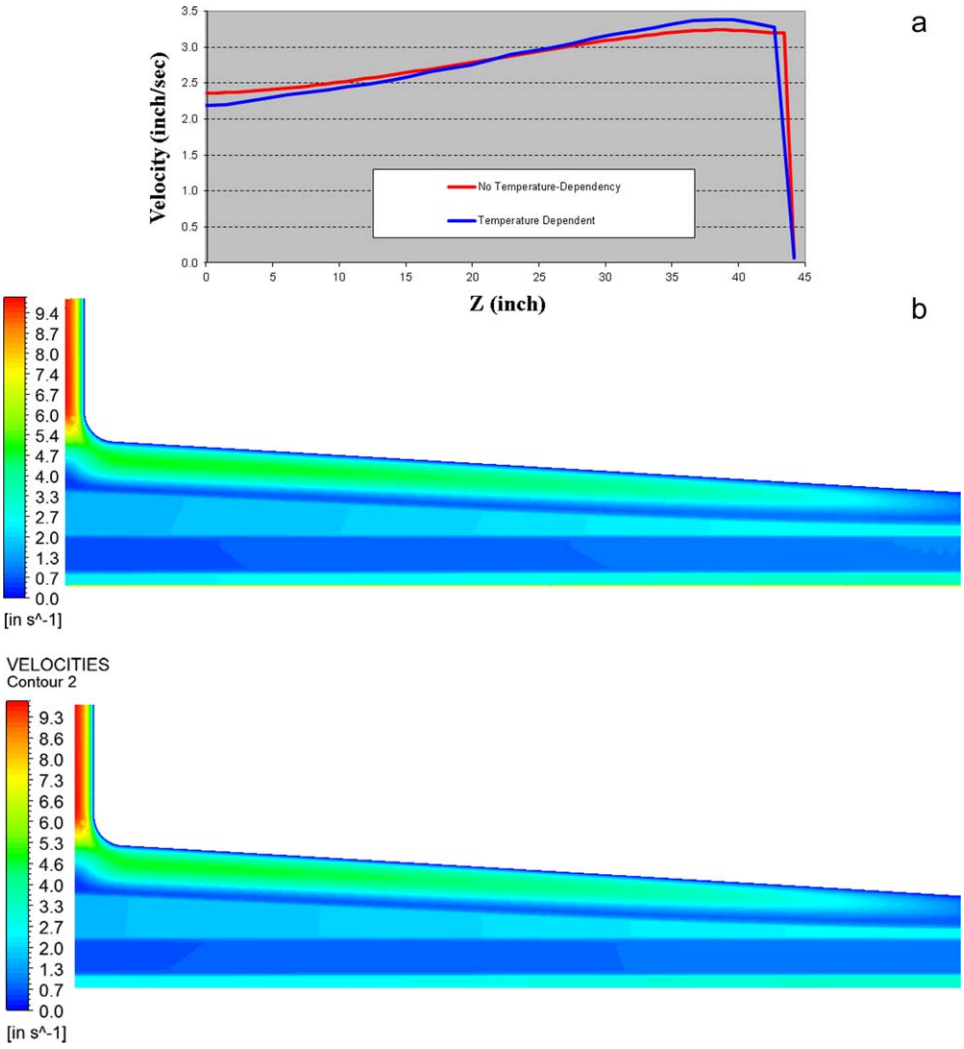

FIG. 20. (a) V-center, (b) V-center $H(t)$ and V-center $H = 1$. [Color figure can be viewed in the online issue, which is available at wileyonlinelibrary.com.]

Figures 10–14 and 15 give the real-world conjugate heat transfer results (PBT) for both insulation and heat loss cases. The variation of manifold wall temperature from the conjugate case is 11°F (from 477 to 488°F in Fig. 10a and b) and 15°F (from 472 to 487°F in Fig. 11a and b) for the insulation case and heat loss case, respectively. The body temperature varies from 444 to 488°F in the insulation case (Fig. 14a–c) and from 268 to 487°F in the heat loss case (Fig. 15a–c). Compared with the previous adiabatic cases, here the conjugate temperature change due to viscous shear heating is reduced to about 6°F.

As can be seen from all the above cases, the body temperature around the cartridge heaters or close to the manifold is quite uniform. This is because the cartridge heaters are designed located equally from the manifold wall, and also they are designed close enough to the manifold wall so as to get the maximum heating efficiency, and also because of the high conductivity of the stainless steel from which the body is made.

From the above die body surface temperature solution for each finite element surface, we can compute the heating cost difference between the insulation case and the non-insulation case according to *Eq. 7*. For the conjugate case, it is found that the non-insulation case costs extra 9 KW more heating source than the insulation case.

For the purpose of tough test of the manifold temperature uniformity, the above results do not include temperature-dependency for viscosity, which tends to reduce temperature variation on the manifold wall. This is because that increasing temperature reduces polymer fluid viscosity, thus reduces viscous shear heating. Figure 17 shows a slightly lower temperature with a little bit less variation on the manifold than the case in Fig. 11 where we assume viscosity does not change with temperature. The comparisons of viscosity given in the Figs. 18 and 19 show that the viscosity does change with temperature. This viscosity change with temperature has shown its effect on the velocity field in the present coupled flow and thermal simulation, as seen in Fig. 20a and b.

CONCLUSION

The present detailed 3D finite element conjugate thermal simulation study provides a useful model for thermal analysis of extrusion die. It is concluded that the effect of the contour body shape on the manifold temperature uniformity is negligible, and the viscous shear heating is generally low. It is also confirmed that the body cartridge heaters should be located equally away from the manifold wall within a close enough distance in order to keep temperature uniformity on the manifold wall. The results show that the flow velocity distribution particularly at the lip exit does change with the flow temperature mainly due to viscosity change in the flow field.

ACKNOWLEDGMENTS

The CAD file of the sample extrusion die was provided by Engineering Department of Nordson EDI.

REFERENCES

1. W. Michaelli, Extrusion Dies for Plastics and Rubber, Hanser, New York (1992).
2. P. Lin and Y. Jaluria, *Polym. Eng. Sci.*, **37**, 1582 (1997).
3. *ANSYS POLYFLOW*, Version14.0, ANSYS (2012).
4. A. Bejan, Convection Heat Transfer, Wiley, New York (1984).

 DOI 10.1002/pen